Chronic nitrogen legacy in the aquifers of China

Xin Liu[1,2], Fu-Jun Yue[1,3*], Li Li[4], Feng Zhou[5,6], Hang Wen[1], Zhifeng Yan[1], Lichun Wang[1], Wei Wen Wong[2], Cong-Qiang Liu[1,3,7], Si-Liang Li[1,3,7*]

[1] Institute of Surface-Earth System Science, School of Earth System Science, Tianjin University, Tianjin, China

[2] Water Studies, School of Chemistry, Monash University, Clayton 3800, Victoria, Australia

[3] Tianjin Key Laboratory of Earth Critical Zone Science and Sustainable Development in Bohai Rim, Tianjin University, Tianjin, China

[4] Department of Civil and Environmental Engineering, The Pennsylvania State University, University Park, PA, USA

[5] Laboratory for Earth Surface Processes, Ministry of Education, College of Urban and Environmental Sciences, Peking University, Beijing, China

[6] College of Geography and Remote Sensing, Hohai University, Nanjing, P.R. China

[7] Haihe Laboratory of Sustainable Chemical Transformations, Tianjin, China

*Corresponding author: Dr. Fu-Jun Yue, fujun_yue@tju.edu.cn;

Dr. Si-Liang Li, siliang.li@tju.edu.cn;

This PDF file includes:

1. Supplementary Figures. S1 to S14

Fig. S1 The relationship between vadose zone depth and nitrate concentration in North Coast (NC) and South West (SW). (a) The relationship between Lg(GW depth + 1) and Lg(NO_3^-) in North Coast. (b) Correlations between Lg(GW depth + 1) and Lg(NO_3^-) in South West.

Fig. S2 The relationship between Eh and (a) NO_3^- and (b) DOC values in Chinese groundwater.

Fig. S3 Relationship between nitrate concentration and its isotopes in wells at different depths. (a-d) The isotopic composition of $\delta^{15}N$-NO_3^- and $\delta^{18}O$-NO_3^- values are utilized to identify potential NO_3^- sources, with typical range of isotope sources adapted from Carrey, et al. [1] and Kendall, et al. [2]. Mixing processes are illustrated by $\delta^{15}N$-NO_3^- and 1/NO_3^- (e-h), while removal process (including denitrification or assimilation) are demonstrated through $\delta^{15}N$-NO_3^- versus Ln(NO_3^-) (i-l).

Fig. S4 Sankey diagram displaying the synchronous distribution of class I and II wells in differential ecoregion, population density, land use, and nitrate.

Fig. S5 Responses of well water nitrate concentration to inputs of (a) agricultural N fertilizer, (b) TN wastewater, and (c) ammonia wastewater in different economic regions. The data were obtained from the National Bureau of Statistics of the People's Republic of China (http://www.stats.gov.cn) and averaged over the last two decades.

Fig. S6 Trend of agricultural N fertilizer usage, and the discharge of TN wastewater, and ammonia wastewater from 2000 to 2020. Blue hexagon, yellow quadrilateral, and green circle represent agricultural N fertilizer (left-Y axis), TN wastewater (right-Y axis), and ammonia wastewater (right-Y axis), respectively. The data were obtained from the National Bureau of Statistics of the People's Republic of China (http://www.stats.gov.cn).

Fig. S7 The relationship between $\delta^{15}N\text{-}NO_3^-$ and $\delta^{18}O\text{-}NO_3^-$ values in Chinese groundwater. Apart from the study by Yang, et al. [3], there is a clear positive correlation between $\delta^{15}N\text{-}NO_3^-$ and $\delta^{18}O\text{-}NO_3^-$ values in Chinese groundwater, indicating that denitrification plays a significant role in this context. Meanwhile, Yang, et al. [3] also noted that the region is substantially influenced by denitrification. Therefore, it can be concluded that nitrogen removal in Chinese groundwater is primarily controlled by denitrification processes.

Fig. S8 Spatial patterns of nitrate concentration at different groundwater depth. (a) GW depth < 20m. (b) 20 ≤ GW depth < 50 m. (c) 50 ≤ GW depth < 100 m. (d) GW depth ≥ 100 m. The nitrate concentrations were grouped into 17 categories to generate a color gradient, where light and dark colors represent low and high values, respectively.

Fig. S9 The country was divided into eight regions based on economic regions based on the economic development and geographical conditions. North Coast (NC, including Beijing, Hebei province, Shandong province, and Tianjin), Middle of Yellow River (MYR, including Henan province, Inner Mongolia, Shaanxi province, and Shanxi province), North East (NE, including Heilongjiang province, Jilin province, and

Liaoning province), South West (SW, including Chongqing, Guangxi province, Guizhou province, Sichuan province, and Yunnan province), East Coast (EC, including Anhui province, Jiangsu province, and Zhejiang province), North West (NW, including Gansu province, Ningxia province, Qinghai province, Tibet, and Xinjiang province), Middle of Changjiang River (MCR, including Hubei province, Hunan province, and Jiangxi province), South Coast (SC, including Fujian province, Guangdong province, Hainan province, Hongkong, Macao, and Taiwan province).

Fig. S10 Spatial distribution of elevation in China. The elevation dataset was provided by the Ecological Forecasting Lab of National Aeronautics and Space Administration (NASA) Ames Research Center (http://ecocast.arc.nasa.gov/) with a spatial resolution of 1 km × 1 km.

Fig. S11 The spatial distribution of different land use types, including natural (forest, grassland, waters, and others), cropland (cropland), and urban (settlement). The data were provided by the Data Center for Resources and Environmental Sciences, Chinese Academy of Sciences (RESDC) (http://www.resdc.cn) with a spatial resolution of 1 km × 1 km.

Fig. S12 The Map of China showing the population density (person km^{-2}) and the "Hu Huangyong" Line. The "Hu Huanyong" Line is known as a Chinese geographic boundary between the less-developed and sparsely-populated Western area and the high-developed and densely-populated Eastern area[3]. The data were provided by the Data Center for Resources and Environmental Sciences, Chinese Academy of Sciences

(RESDC) (http://www.resdc.cn) with a spatial resolution of 1 km × 1 km.

Fig. S13 Spatial pattern of mean annual precipitation values for the period 1982 ~ 2015. The data were obtained from the China Meteorological Administration (CMA) (http://data.cma.cn/) with a spatial resolution of 0.25° × 0.25°.

Fig. S14 The Map of China showing mean annual temperature values for the period 1982 ~ 2015. The data were obtained from the China Meteorological Administration (CMA) (http://data.cma.cn/) with a spatial resolution of 0.25° × 0.25°.

2. Supplementary Tables S1 to S6

Table S1. The variations of nitrate and its isotopes state at different groundwater depths and ecoregions.

Table S2. Spatially continuous environmental variables considered in the analysis and prediction of nitrate concentrations in groundwater. The relative importance of 66 variables for groundwater nitrate concentrations was determined by regression forecasting using random forests. The columns marked * ($P < 0.05$) and ** ($P < 0.01$) represent drivers have significant impacts on nitrate concentrations; at the equator, 30” is approximately equal to 1 km; “−” represents no unit.

Table S3. Isotopic composition of four potential NO_3^- end-members used in MixSIAR model.

Table S4. Proportional contribution of nitrate sources of different groundwater depths estimated using MixSIAR model.

Table S5. Numbers of samples in different economic zones from 2000 to 2020 (N = 3163). Note: some groundwater sampling sites do not directly provide sampling time.

Table S6. Numbers and proportion of samples in different categories of groundwater depths, location, ecoregions, land use types, and population density.

1. Supplementary Figures

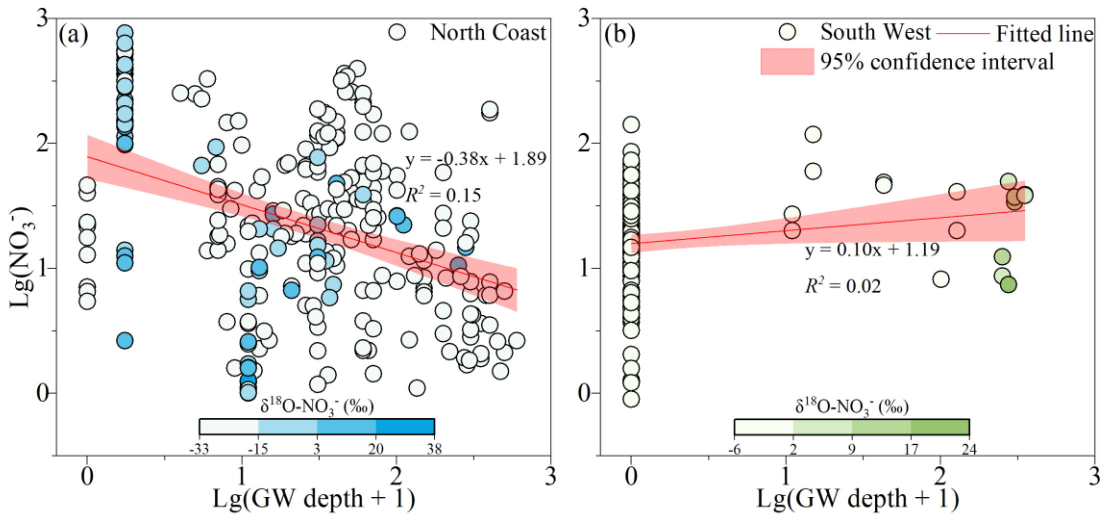

Fig. S1 The relationship between vadose zone depth and nitrate concentration in North Coast (NC) and South West (SW). (a) The relationship between Lg(GW depth + 1) and Lg(NO_3^-) in North Coast. (b) Correlations between Lg(GW depth + 1) and Lg(NO_3^-) in South West.

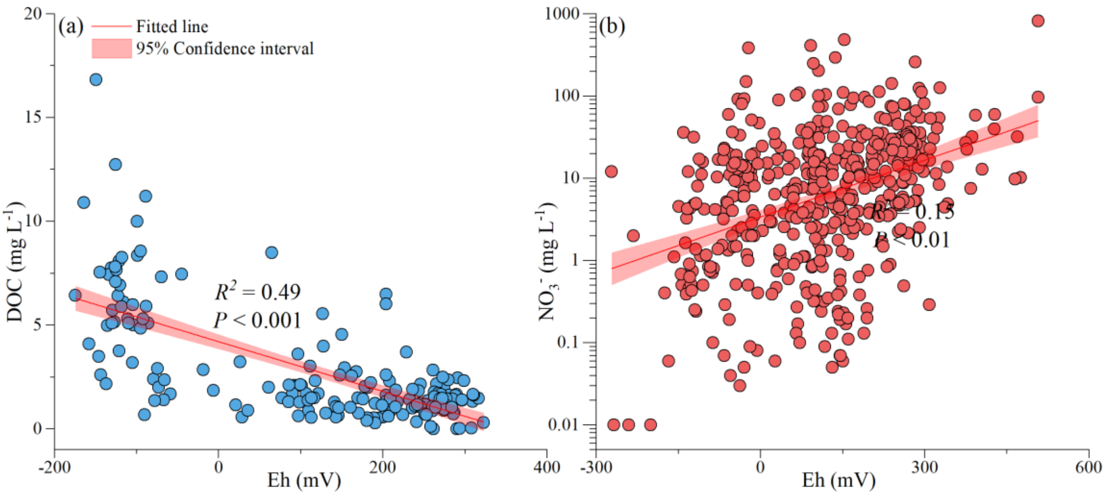

Fig. S2 The relationship between Eh and (a) NO_3^- and (b) DOC values in Chinese groundwater.

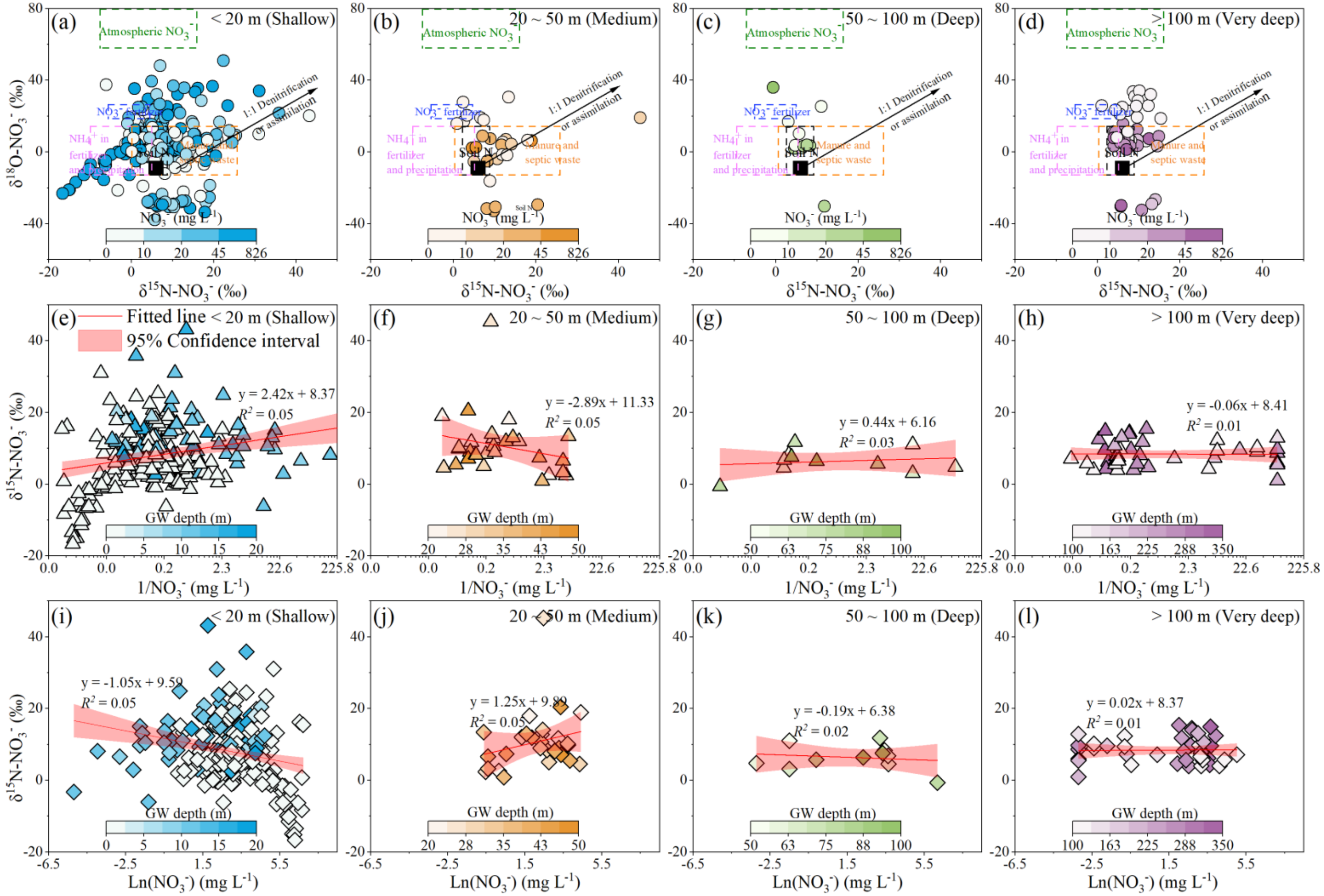

Fig. S3 Relationship between nitrate concentration and its isotopes in wells at different depths. (a-d) The isotopic composition of $\delta^{15}N\text{-}NO_3^-$ and

$\delta^{18}O$-NO_3^- values are utilized to identify potential NO_3^- sources, with typical range of isotope sources adapted from Carrey, et al. [1] and Kendall, et al. [2]. Mixing processes are illustrated by $\delta^{15}N$-NO_3^- and $1/NO_3^-$ (e-h), while removal process (including denitrification or assimilation) are demonstrated through $\delta^{15}N$-NO_3^- versus $Ln(NO_3^-)$ (i-l).

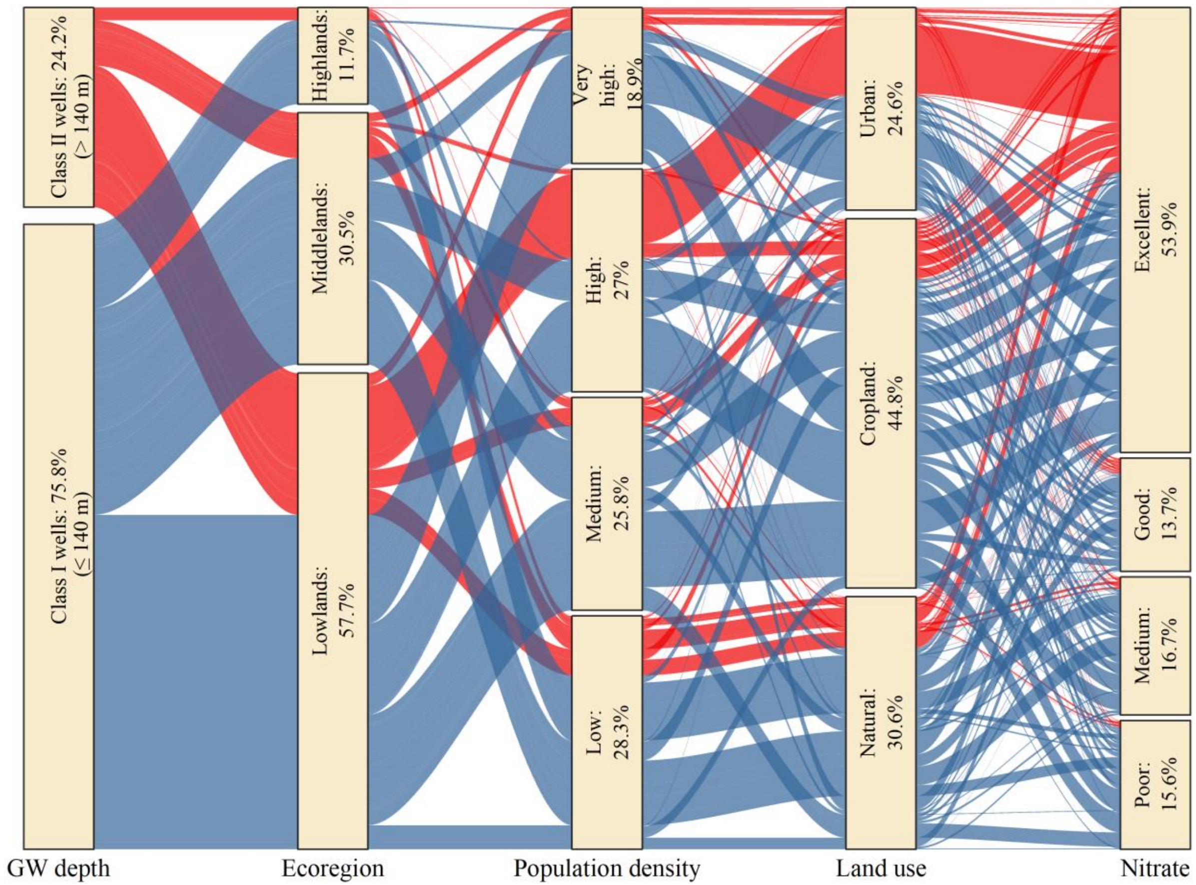

Fig. S4 Sankey diagram displaying the synchronous distribution of class I and II wells in differential ecoregion, population density, land use, and nitrate.

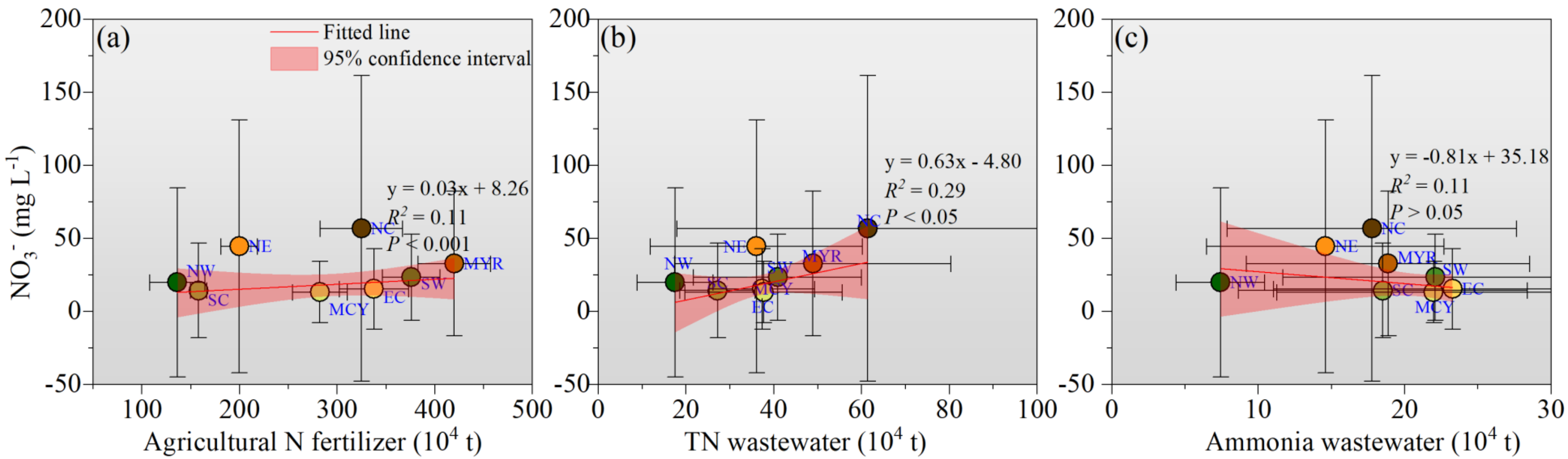

Fig. S5 Responses of well water nitrate concentration to inputs of (a) agricultural N fertilizer, (b) TN wastewater, and (c) ammonia wastewater in different economic regions. The data were obtained from the National Bureau of Statistics of the People's Republic of China (http://www.stats.gov.cn) and averaged over the last two decades.

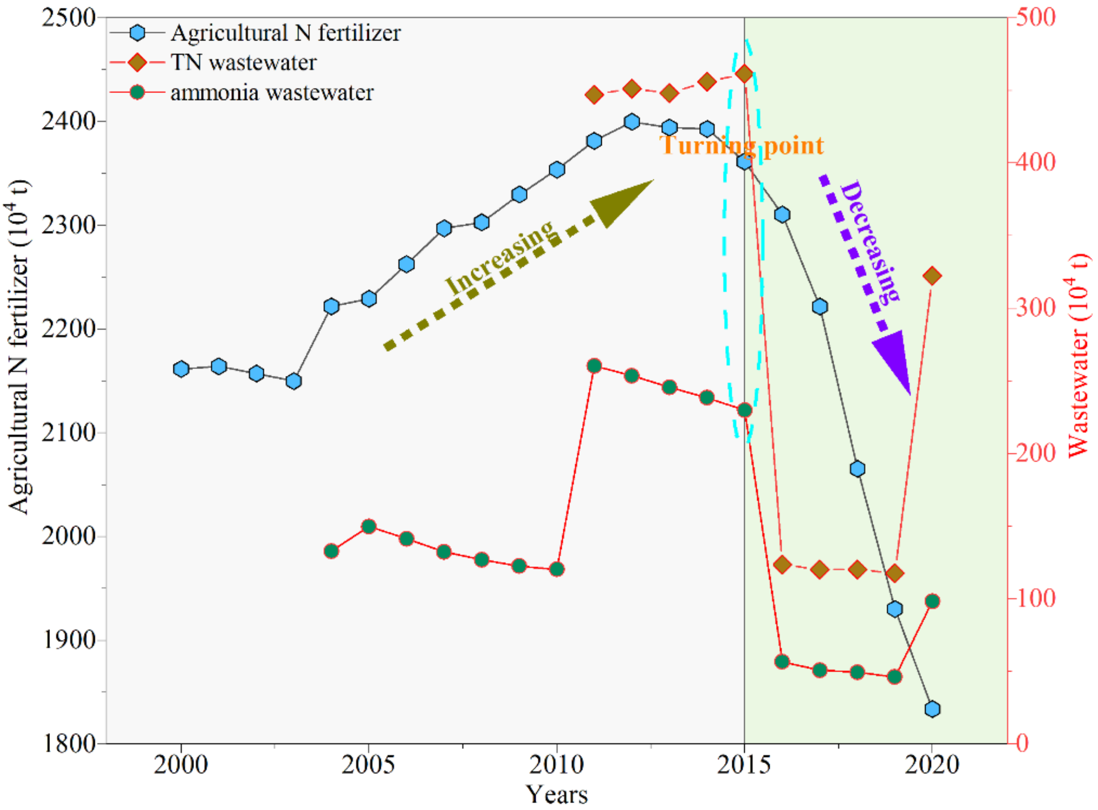

Fig. S6 Trend of agricultural N fertilizer usage, and the discharge of TN wastewater, and ammonia wastewater from 2000 to 2020. Blue hexagon, yellow quadrilateral, and green circle represent agricultural N fertilizer (left-Y axis), TN wastewater (right-Y axis), and ammonia wastewater (right-Y axis), respectively. The data were obtained from the National Bureau of Statistics of the People's Republic of China (http://www.stats.gov.cn).

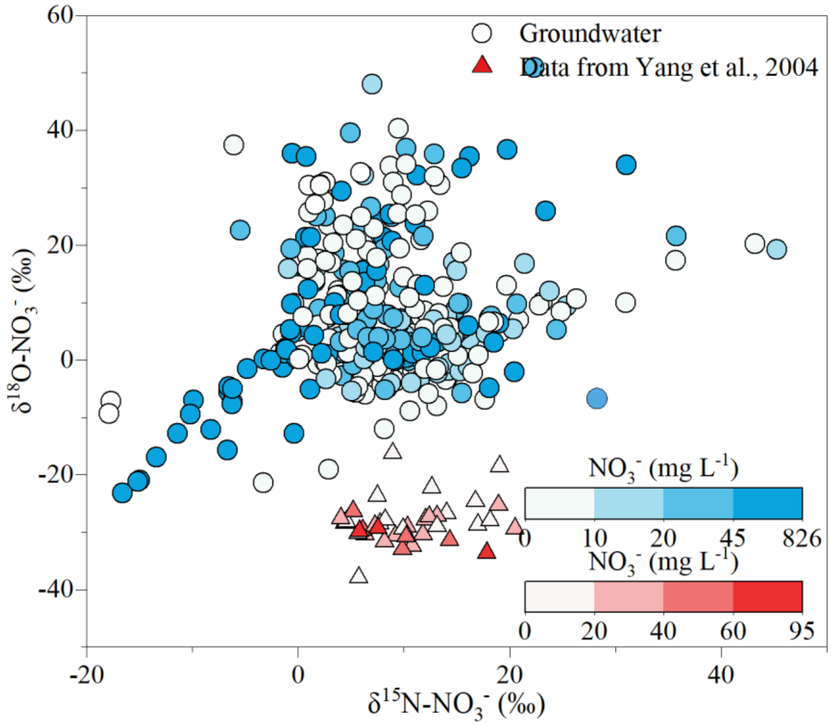

Fig. S7 The relationship between $\delta^{15}N\text{-}NO_3^-$ and $\delta^{18}O\text{-}NO_3^-$ values in Chinese groundwater. Apart from the study by Yang, et al. [3], there is a clear positive correlation between $\delta^{15}N\text{-}NO_3^-$ and $\delta^{18}O\text{-}NO_3^-$ values in Chinese groundwater, indicating that denitrification plays a significant role in this context. Meanwhile, Yang, et al. [3] also noted that the region is substantially influenced by denitrification. Therefore, it can be concluded that nitrogen removal in Chinese groundwater is primarily controlled by denitrification processes.

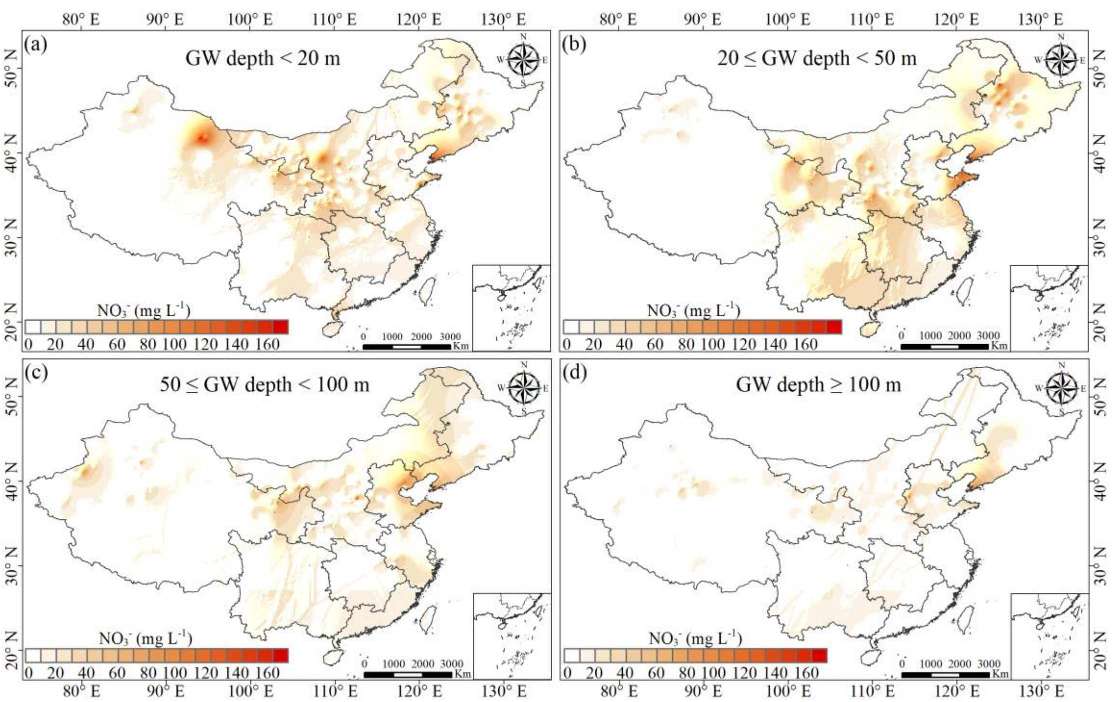

Fig. S8 Spatial patterns of nitrate concentration at different groundwater depth. (a) GW depth < 20m. (b) 20 ≤ GW depth < 50 m. (c) 50 ≤ GW depth < 100 m. (d) GW depth ≥ 100 m. The nitra te concentrations were grouped into 17 categories to generate a color gradient, where light and dark colors represent low and high values, respectively.

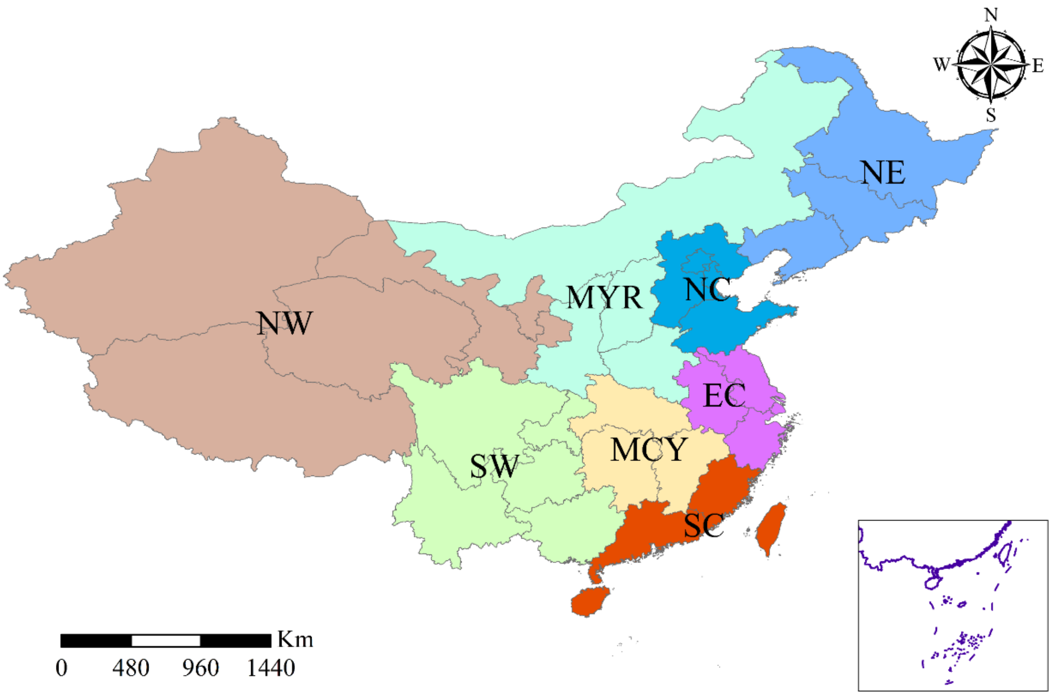

Fig. S9 The country was divided into eight regions based on economic regions based on the economic development and geographical conditions. North Coast (NC, including Beijing, Hebei province, Shandong province, and Tianjin), Middle of Yellow River (MYR, including Henan province, Inner Mongolia, Shaanxi province, and Shanxi province), North East (NE, including Heilongjiang province, Jilin province, and Liaoning province), South West (SW, including Chongqing, Guangxi province, Guizhou province, Sichuan province, and Yunnan province), East Coast (EC, including Anhui province, Jiangsu province, and Zhejiang province), North West (NW, including Gansu province, Ningxia province, Qinghai province, Tibet, and Xinjiang province), Middle of Changjiang River (MCR, including Hubei province, Hunan province, and Jiangxi province), South Coast (SC, including Fujian province, Guangdong province, Hainan province, Hongkong, Macao, and Taiwan province).

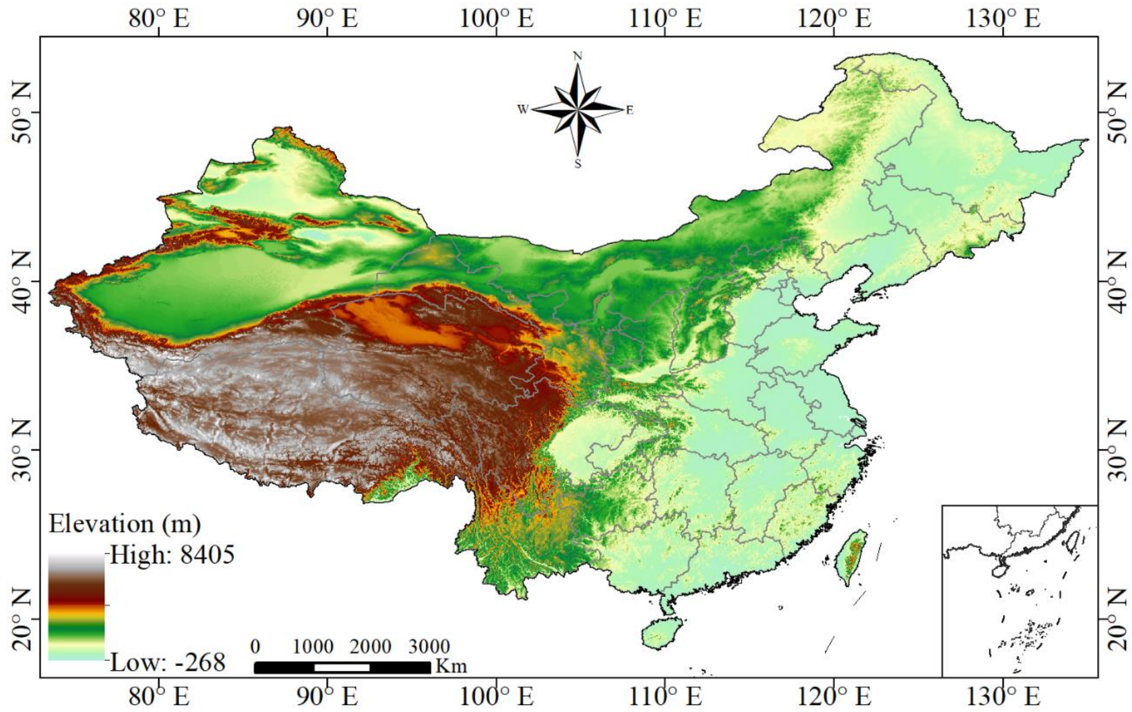

Fig. S10 Spatial distribution of elevation in China. The elevation dataset was provided by the Ecological Forecasting Lab of National Aeronautics and Space Administration (NASA) Ames Research Center (http://ecocast.arc.nasa.gov/) with a spatial resolution of 1 km × 1 km.

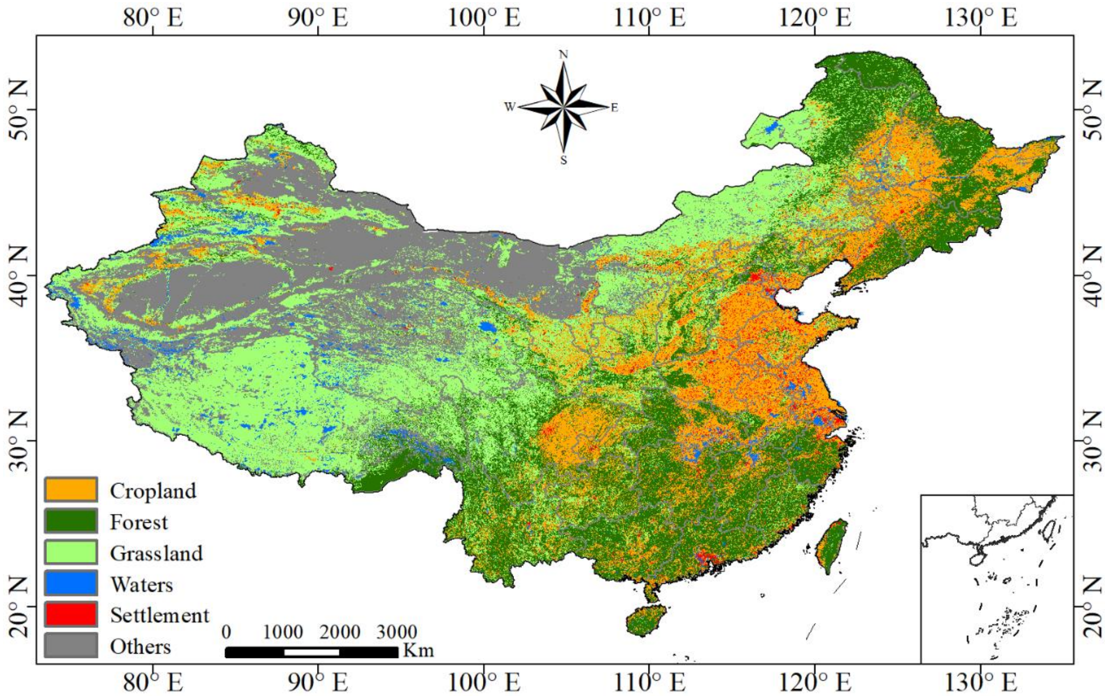

Fig. S11 The spatial distribution of different land use types, including natural (forest, grassland, waters, and others), cropland (cropland), and urban (settlement). The data were provided by the Data Center for Resources and Environmental Sciences, Chinese Academy of Sciences (RESDC) (http://www.resdc.cn) with a spatial resolution of 1 km × 1 km.

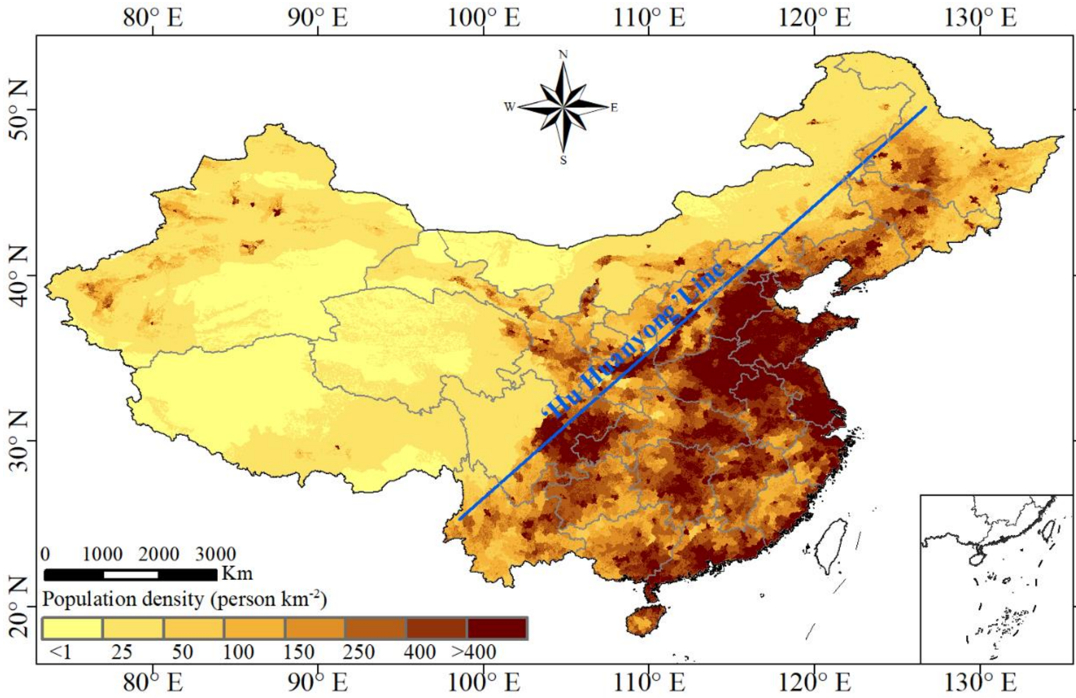

Fig. S12 The Map of China showing the population density (person km^{-2}) and the "Hu Huangyong" Line. The "Hu Huanyong" Line is known as a Chinese geographic boundary between the less-developed and sparsely-populated Western area and the high-developed and densely-populated Eastern area[3]. The data were provided by the Data Center for Resources and Environmental Sciences, Chinese Academy of Sciences (RESDC) (http://www.resdc.cn) with a spatial resolution of 1 km × 1 km.

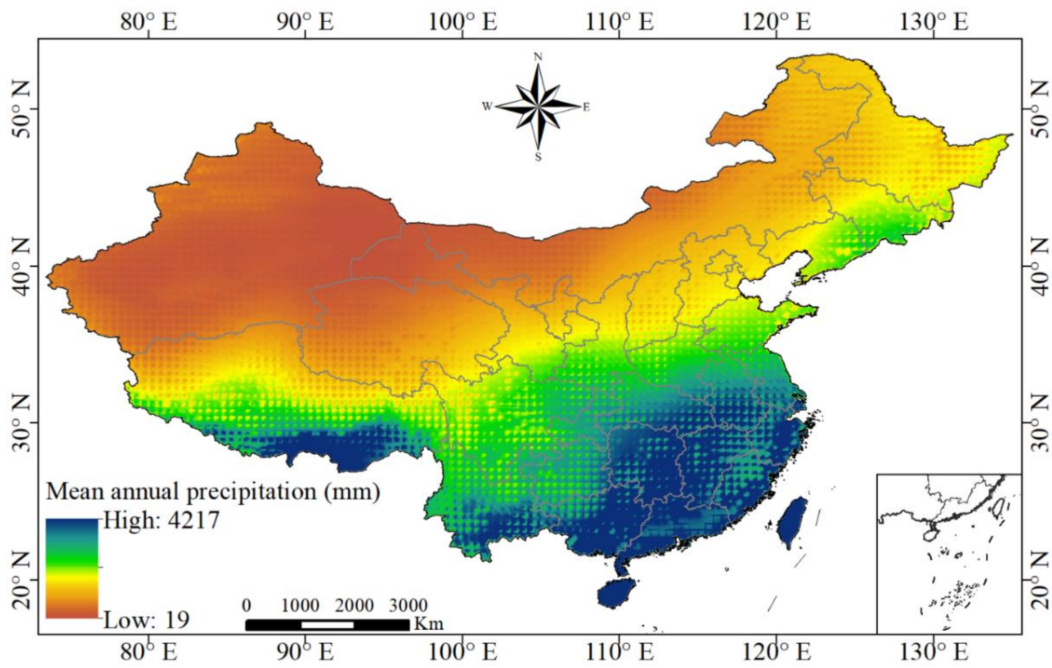

Fig. S13 Spatial pattern of mean annual precipitation values for the period 1982 ~ 2015. The data were obtained from the China Meteorological Administration (CMA) (http://data.cma.cn/) with a spatial resolution of 0.25° × 0.25°.

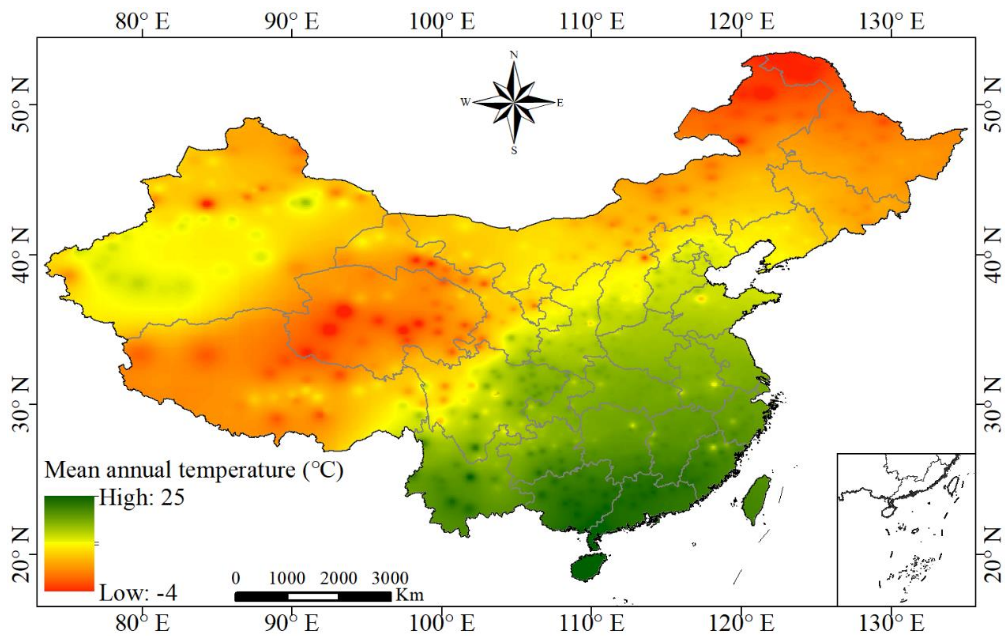

Fig. S14 The Map of China showing mean annual temperature values for the period 1982 ~ 2015. The data were obtained from the China Meteorological Administration (CMA) (http://data.cma.cn/) with a spatial resolution of 0.25° × 0.25°.

2. Supplementary Tables

Table S1. The variations of nitrate and its isotopes state at different groundwater depths and ecoregions.

See supplementary .xlsx file available https://doi.org/10.6084/m9.figshare.28103579.

Table S2. Spatially continuous environmental variables considered in the analysis and prediction of nitrate concentrations in groundwater. The relative importance of 66 variables for groundwater nitrate concentrations was determined by regression forecasting using random forests. The columns marked * ($P < 0.05$) and ** ($P < 0.01$) represent drivers have significant impacts on nitrate concentrations; at the equator, 30” is approximately equal to 1 km; “−” represents no unit.

See supplementary .xlsx file available https://doi.org/10.6084/m9.figshare.28103579.

Table S3. Isotopic composition of four potential NO_3^- end-members used in MixSIAR model.

See supplementary .xlsx file available https://doi.org/10.6084/m9.figshare.28103579.

Sources	$\delta^{15}N\text{-}NO_3^-$		$\delta^{18}O\text{-}NO_3^-$	
	Mean	SD	Mean	SD
Atmospheric Deposition	4.6	3.9	54	13.2
Soil Nitrogen	7.5	5.23	-2.0	8.0
Manure & Sewage	15.0	1.2	-2.0	8.0
Chemical Fertilizer	0.0	1.4	-2.3	0.6

Data obtained from Liu, et al. [4], Ren, et al. [5], Black and Waring [6], Choi, et al. [7], Curt, et al. [8], Ding, et al. [9], Zong, et al. [10], Yu, et al. [11].

Table S4. Proportional contribution of nitrate sources of different groundwater depths estimated using MixSIAR model.

See supplementary .xlsx file available https://doi.org/10.6084/m9.figshare.28103579.

Table S5. Numbers of samples in different economic zones from 2000 to 2020 (N = 3163). Note: some groundwater sampling sites do not directly provide sampling time.

See supplementary .xlsx file available https://doi.org/10.6084/m9.figshare.28103579.

Table S6. Numbers and proportion of samples in different categories of groundwater depths, location, ecoregions, land use types, and population density.

See supplementary .xlsx file available https://doi.org/10.6084/m9.figshare.28103579.

References

1 Carrey, R. *et al.* Combining multi-isotopic and molecular source tracking methods to identify nitrate pollution sources in surface and groundwater. *Water Res.* **188**, 116537, (2021).

2 Kendall, C., Elliot, E. M. & Wankel, S. D. Tracing anthropogenic inputs of nitrogen to ecosystems. *In: Michener, R., Lajtha, K. (Eds.), Stable Isotopes in Ecology and Environmental Science, second ed. Blackwell Publishing Ldt, Oxford, pp. 375-449*. (2007).

3 Yang, Y., Cai, H., Liu, C. & Zhou, A. The application of isotopes ^{15}N and ^{18}O in NO_3^- technique in the study on nitrogen contamination to groundwater in karst area-A case study on the high incident region of esophagus cancer in Linzhou, Henan, China. *Crsologica Sinica* **23**, 40-46. (In Chinese), (2004).

4 Liu, X., Yue, F. J., Wong, W. W., Guo, T. L. & Li, S. L. Unravelling nitrate transformation mechanisms in karst catchments through the coupling of high-frequency sensor data and machine learning. *Water Res.* **267**, 122507, (2024).

5 Ren, X., Yue, F. J., Tang, J., Li, C. & Li, S. L. Nitrate transformation and source tracking of rivers draining into the Bohai Sea using a multi-tracer approach combined with an optimized Bayesian stable isotope mixing model. *J. Hazard. Mater.* **463**, 132901, (2023).

6 Black, A. & Waring, S. The natural abundance of ^{15}N in the soil water system of a small catchment area. *Soil Res.* **15**, 51, (1977).

7 Choi, W. J., Chang, S. X. & Hao, X. White spruce response to co-composted hydrocarbon-contaminated drilling waste: Effects of compost age and nitrogen fertilization. *Journal Environmental Quality* **34**, 1319-1327, (2005).

8 Curt, M. D., Aguado, P., Sánchez, G., Bigeriego, M. & Fernández, J. Nitrogen

isotope ratios of synthetic and organic sources of nitrate water contamination in Spain. *Water, Air, and Soil Pollution* **151**, 135-142, (2004).

9 Ding, J. *et al.* Identifying diffused nitrate sources in a stream in an agricultural field using a dual isotopic approach. *Sci. Total Environ.* **484**, 10-18, (2014).

10 Zong, Z. *et al.* First assessment of NO_x sources at a regional background site in north China using isotopic analysis linked with modeling. *Environ. Sci. Technol.* **51**, 5923-5931, (2017).

11 Yu, J. *et al.* Dual-isotope-based source apportionment of nitrate in 30 rivers draining into the Bohai Sea, north China. *Environ. Pollut.* **283**, 117112, (2021).